Naval Research Laboratory
Washington, DC 20375-5320

NRL/MR/6410--04-8840

The Influence of Fin Rigidity on the Force Production in the Bird-Wrasse: A Computational Study

RAVI RAMAMURTI
WILLIAM C. SANDBERG
Laboratory for Computational Physics and Fluid Dynamics

November 10, 2004

REPORT DOCUMENTATION PAGE

Form Approved
OMB No. 0704-0188

1. REPORT DATE *(DD-MM-YYYY)*	2. REPORT TYPE	3. DATES COVERED *(From - To)*
10-11-2004	Memorandum	

4. TITLE AND SUBTITLE

The Influence of Fin Rigidity on the Force Production in the Bird-Wrasse: A Computational Study

5a. CONTRACT NUMBER

5b. GRANT NUMBER
64-1530-0-4

5c. PROGRAM ELEMENT NUMBER

6. AUTHOR(S)

Ravi Ramamurti and William C. Sandberg

5d. PROJECT NUMBER

5e. TASK NUMBER

5f. WORK UNIT NUMBER

7. PERFORMING ORGANIZATION NAME(S) AND ADDRESS(ES)

Naval Research Laboratory, Code 6410
4555 Overlook Avenue, SW
Washington, DC 20375-5320

8. PERFORMING ORGANIZATION REPORT NUMBER

NRL/MR/6410--04-8840

9. SPONSORING / MONITORING AGENCY NAME(S) AND ADDRESS(ES)

10. SPONSOR / MONITOR'S ACRONYM(S)

11. SPONSOR / MONITOR'S REPORT NUMBER(S)

12. DISTRIBUTION / AVAILABILITY STATEMENT

Approved for public release; distribution is unlimited.

13. SUPPLEMENTARY NOTES

14. ABSTRACT

The three-dimensional unsteady computations of fish swimming with oscillating and deforming fins of varying rigidity were carried out. The objective of these variable rigidity computations was to investigate the importance of fin deformation of the fluid dynamics of force production. An unstructured grid-based unsteady Navier-Stokes solver with automatic adaptive remeshing was used to compute the flow about the wrasse through several complete cycles of pectoral fin oscillation for each of the fins studied. The computations show that when the fin is made rigid by specifying the motion with just the leading edge of the fin tip, the thrust produced during the upstroke is less than half of the peak thrust produced by the flexible cases. During the downstroke, the rigid fin and the fin with the motion prescribed with only the leading and trailing edges produced no positive thrust, while all the flexible cases considered reproduced the thrust production of the fully deformable fin. In the case of the rigid fin, there is a substantial penalty in lift during the upstroke.

15. SUBJECT TERMS

Bird-wrasse; Flapping foil; Deforming fin; Incompressible flow; Unstructured grid

16. SECURITY CLASSIFICATION OF:			17. LIMITATION OF ABSTRACT	18. NUMBER OF PAGES	19a. NAME OF RESPONSIBLE PERSON
a. REPORT	b. ABSTRACT	c. THIS PAGE			Ravi Ramamurti
Unclassified	Unclassified	Unclassified	UL	21	19b. TELEPHONE NUMBER *(include area code)* (202)-767-0608

Standard Form 298 (Rev. 8-98)
Prescribed by ANSI Std. Z39.18

Table of Contents

List of Figures

The influence of fin rigidity on the force production in the Bird-Wrasse: A computational study

INTRODUCTION

Many fishes that swim with paired pectoral fins use fin stroke parameters that produce thrust force from lift in powering their underwater flight. Flapping locomotion mechanisms are of interest to behavioral biologists, biomechanics researchers, and engineers attempting to develop systems that can match the performance of the living creatures. One question that arises in investigating the mechanisms responsible for the high thrust/lift generation in flapping locomotion is the importance of chordwise and spanwise deformation. Flapping foil propulsion has also received considerable attention in the past few years as an alternative to the propeller. This mode of propulsion which involves no body undulation, has many applications, such as submersibles propulsion, maneuvering, position-keeping and flow control which are of interest to the Unmanned Underwater Vehicle (UUV) hydrodynamic community and unconventional aerodynamics of Micro Aerial Vehicles (MAV) for the aerodynamic community. For both types of vehicles, it is important to accurately quantify the performance benefits of flexible wings, since providing the flexibility is a major technical challenge.

Dickinson et al. (1999) has studied the effects of the wing rotation in the fruitfly, *Drosophila,* and Walker and Westneat (1997) have studied the kinematics of the fin motion in a class of fishes, namely the bird wrasse, experimentally. Three dimensional unsteady flow computations over insects have been carried out by Liu and Kawachi (1998) who obtained qualitative agreement for the flow patterns over a hovering hawkmoth with the windtunnel visualizations of Willmott and Ellington (1997). Ramamurti and Sandberg have studied the force production in *Drosophila* (2002a) and in a swimming bird wrasse fish (2002b) computationally and obtained good agreement with experimental results with measured force data of Dickinson et al. (1999) and the fish acceleration data of Walker and Westneat (1997).

In this study, we continue our computational investigations on flapping fin and wing flows for non-undulating bodies. The primary objective in this work is to investigate the fluid dynamics underlying the generation of forces during pectoral fin oscillation as fin rigidity is varied.

THE INCOMPRESSIBLE FLOW SOLVER

The governing equations employed are the incompressible Navier-Stokes equations in Arbitrary Lagrangian-Eulerian (ALE) formulation which are written as

$$\frac{d\mathbf{v}}{dt} + \mathbf{v}_a \cdot \nabla \mathbf{v} + \nabla p = \nabla \cdot \sigma, \tag{1}$$

$$\nabla \cdot \mathbf{v} = 0, \tag{2}$$

where p denotes the pressure, $\mathbf{v}_a = \mathbf{v} - \mathbf{w}$ the advective velocity vector, where $\mathbf{v}$ is the flow velocity and $\mathbf{w}$ is the mesh velocity w and the material derivative is with respect to the mesh velocity $\mathbf{w}$. Both the pressure p and the stress tensor σ have been normalized by the (constant) density ρ and are discretized in time using an implicit time stepping procedure. Thus the equations are Eulerian for zero mesh velocity and Lagrangian if the mesh velocity is the same as

Manuscript approved September 30, 2004.

the flow velocity. The present time-accurate flow solver is discretized in space using a Galerkin procedure with linear tetrahedral elements. The details of the flow solver have already been discussed extensively elsewhere (Ramamurti *et. al.* 1992, 1994, 1995, 1999) in connection with successfully validated solutions for numerous 2-D and 3-D, laminar and turbulent, steady and unsteady flow problems.

RESULTS AND DISCUSSION

The 3-D surface coordinates of the bird-wrasse, *G. varius*, and the kinematics of the flapping pectoral fin were obtained from Walker and Westneat (1997). In that work, the computations were performed using 14 control points to describe the motion of the deforming fin. The motion of these control points were obtained from three distal markers and smoothed using a quintic spline function (Walker, 1998). The procedure for using this data in a computational investgation has been described in detail by Ramamurti et al. (2002). In order to carry out computations of the flow about oscillating and deforming geometries, an unstructured mesh with adaptive remeshing is employed. The mesh movement algorithm is briefly summarized here. First, the Cartesian coordinates on the fin surface were then transformed to a parametric space. The coordinates of the surface points were maintained to be constant in the parametric space throughout the computation while the Cartesian coordinates were computed according to the prescribed motion of the control points. 3-D Unsteady computations of Ramamurti et al (2002b) about the deforming pectoral fins using this experimentally measured fin kinematics were found to give excellent agreement both in the time history of force production throughout the flapping strokes and also the magnitudes of the generated forces.

In the present work, a set of unsteady computations is carried for several cycles of the fin oscillation for fins of varying rigidity, using the incompressible flow solver described above. The rigidity of the fin is varied by selecting a reduced number of control points. Figure 1 shows the control points along the fin tip at the instant when the fin is fully spread out from the body. All the 14 control points that were supplied from experimental observation are shown in Fig. 1A. We can construct a fin that is rigid by using only one control point at the leading edge of the fin tip and the intersection of the leading and trailing edge rays with the body of the wrasse, as shown in Fig. 1B. The kinematics of this rigid fin follows from the motion of this single control point obtained from the experiments. Using the coordinates of this control point at various instants through the flapping cycle and the location of the root points at the leading and trailing edges, we can obtain the coordinates of the points on the fin tip, so that they lie on a plane. Next, the trailing edge point was added to the list of control points as shown in Fig 1C and another point was added at mid-chord along the fin tip. The resulting initial shape is shown in Fig. 1D. Finally, four control points were chosen out of the original 14, such that the leading edge curvature of the fin is defined properly. The points that were chosen are the leading edge and two successive points close to the leading edge and the trailing edge point. The resulting shape is shown in Fig. 1E.

Unsteady Computations

Unsteady simulations were carried out with the bird-wrasse swimming at 45 cm/s so that we may compare the force production of the reduced flexibility cases with earlier computations for the fully deformable fin. The stroke amplitude is approximately 2.14 radians and the frequency of fin oscillation is 3.3 Hz for all configurations, resulting in a mean tip speed of approximately 50 cm/s. Computations were carried out for more than 4 cycles of fin oscillation using a computational mesh consisting of approximately 150K points and 840K tetrahedral elements, for the four modified fin shapes. The time-varying 3-D lift and thrust, computed by integrating the surface pressure over the wrasse body and fin at each time step throughout the simulation, are shown in Fig. 2.

In the case of the rigid fin, a thrust with a peak value of 0.007 N is produced at the beginning of the downstroke, as shown in Fig. 2A. This is similar to the increase lift just after stroke reversal in the hovering *Drosophila*, reported by Dickinson et al. (1999) and Ramamurti and Sandberg (2002a) and is attributed to the wake capture mechanism. The thrust then quickly drops and a drag force is produced for the remainder of the downstroke. The wake capture peak is absent and no positive thrust is produced during the entire downstroke, in the case of the flexible fin with two control points, namely the leading and trailing edges of the fin tip. In contrast, all the other cases of the partially flexible fins produce the same thrust during the downstroke as the fully deformable fin with motion prescribed by all14 control points, starting near zero at the beginning of the downstroke and increasing to a maximum of 0.008 N at about 30% of the downstroke. During the upstroke, the rigid fin produces a peak thrust of 0.022 N at about 61% of the upstroke, compared to a peak value of 0.046 N produced by the flexible fin at 64% of the upstroke. The flexible fin with two control points achieves a peak value of 0.046 N but at an earlier time, about 47% of the upstroke. The thrust produced in the case of the flexible fin with three control points is very similar to the fully flexible case. If only the leading edge curvature of the fin is retained, as in the case with 4 control points, the peak thrust achieved during the upstroke is 0.0675 N and occurs at approximately 60% and 92% of the upstroke. It is clear that the results using 3 control points matched exactly with the results obtained using all 14 control points. This is to be expected as the motion of the 14 control points in the experiments were derived from these three points. During the downstroke, the lift, shown in Fig. 2B, produced by the flexible fin using 3, 4 and 14 control points attains a peak value of approximately 0.08 N at 37% of the downstroke; a peak lift of 0.123 N is attained at 30% of downstroke with the leading and trailing edge control points and a maximum lift of 0.16 N is attained at about 40% of the downstroke with a fully rigid fin. But, the rigid fin loses the lift during the upstroke with a minimum lift of –0.37 N at about 50% of the upstroke. The minimum lift attained in the case with 2 control points is approximately –0.145 N, which occurs at about 39% of the upstroke, and for the case with 4 control points a minimum lift of –0.104 N is attained at about 43% of the upstroke. Again, the case with 3 control points matches exactly with the fully flexible fin, as expected. These results suggest that the fish or a vehicle with a rigid fin or the fin controlled by just 2 points will experience much larger amplitude vertical excursions than with a flexible fin.

The orientation of the fin at a few instants during one cycle of the fin oscillation is shown in Fig. 3. Figure 4 shows the pressure distribution on the surface of the Bird-wrasse and its fin at t = 0.861 s for the fully flexible fin case and the flexible fin with 4 control points. The orientation

of the fin in both the cases is nearly the same, as can be seen from Fig. 4A and 4D. The pressure is non-dimensionalized with respect to the dynamic head using the mean tip velocity of 50cm s^{-1}. Comparing Fig. 4B and 4E, we can see that the pressure near the leading edge is higher in the 4 control point case and it extends over a wide region on the upper fin surface. From Figs. 4C and 4F, it is also clear the minimum pressure on the lower surface of the fin is considerably lower (darker blue) in the 4 control point case compared to the fully flexible fin, resulting in a larger thrust force. Figure 5 shows the velocity vectors on a plane z = 1.5 cm in the wake of the pectoral fin at t = 0.861 s, which corresponds to nearly the instant at which peak thrust is produced during the upstroke. Although the leading edge curvature is the same in Figs. 5A and 5B, the curvature of the fin in the mid-chord is reduced in the case where only 4 control points were used. This reduces the recirculation both in magnitude and extent on the upper surface of the fin. Hence, the pressure on this surface is higher as shown in Fig. 4F, resulting in a higher thrust.

The increase in thrust production just after the stroke reversal to begin the downstroke, in the rigid fin is investigated next. Figure 6A shows the velocity vectors at an instant where the thrust production reaches a local maximum for the rigid fin. Here, the presence of wake vortices from the previous upstroke in the fin region is clearly evident. These velocity vectors when compared to the case of the fully deformable fin at a similar instant, Fig. 6B, do not show the presence of the upstroke vortices in the fin region. The presence of upstroke vortices also result in an increased pressure, Fig. 6C, near the leading edge approximately 70% of the span away from the root, resulting in an increased thrust at this instant.

Figure 7 shows the orientation of the pectoral fin and the pressure distribution at t = 0.954 s, when the thrust production is minimum for the flexible fin case using 2 control points. At this instant, the pressure distribution on both sides of the fin are shown in Fig. 7B and 7C, for the fully flexible case. Comparing this with the pressure distribution for the case with 2 control point, Figs. 7E and 7F, we see that in both cases, the bottom portion of the fin experiences high pressure near the leading edge. But in the case of the fully flexible fin, the fin at the leading edge tip is oriented in such a manner so as to produce a thrust. Also, in the case of the fin with 2 control points, a large low pressure region forms near the junction of the fin and the body on the upper surface contributing to a drag. The reason for this low pressure region is due to the presence of a large recirculation region seen in Fig. 8. Although the leading and trailing edges in both case are prescribed in the same manner, the curvature in the 2 control point case, Fig 8B, is pronounced in the middle of the fin compared to the fully flexible case, Fig. 8A, leading to a large recirculation, resulting in lower pressure on the upper surface.

The origin of the loss of lift during the upstroke in the case of the rigid fin is due to the increased angle of attack the fin experiences with respect to the resultant forward velocity of the fish and the velocity of the fin. In the case of the fully flexible fin, the fin is flexed concave upwards reducing the angle of attack at the leading edge whereas the flow is directly incident on the upper surface of the rigid fin. This is clear from the pressure distribution on the rigid fin at t= 0.855 s, Fig. 9D and 9E, compared to that of the fully flexible case at a close instant, Figs. 9A and 9B. In both cases, a high pressure region is formed at the leading edge of the fin tip on the upper surface of the fin and lower pressure on the bottom surface, contributing to a downward force. But, the magnitudes of these pressures are much higher in the rigid case, thus producing a

large downward force. In the case of the fully flexible fin, this loss of lift is offset by the upward force in the region close to the body where high pressure exists on the bottom surface and lower pressure on the upper surface. The lower pressure on the upper surface appears due to the presence of a recirculation region at the body junction, shown in Fig. 9C which is absent in the rigid case, Fig. 9F due to the lack of curvature of the fin. Figure 10 shows the pressure distribution on the fully flexible fin (A and B) and the rigid fin (C and D) at an instant close to the maximum lift production during the downstroke. Again, the lower side of the fin has higher pressure with the rigid fin experiencing larger magnitude of pressure difference, producing a larger lift.

SUMMARY AND CONCLUSIONS

We computed the unsteady dynamics about a bird wrasse with flapping and deforming pectoral fins using a new moving mesh capability for unstructured adaptive meshes. The unsteady computations using the prescribed kinematics of the pectoral fin have been compared experimental results. By selecting a reduced number of control points used to define the fin kinematics, the rigidity of the fin was varied. Several unsteady computations were performed fro various rigidity of the fin ranging from a fully rigid to a fully deformable fin. We found that when the fin is made rigid by specifying the motion with just the leading edge of the fin tip, the thrust produced during the upstroke is less than half of the peak thrust produced by the flexible cases. The rigid fin and the fin with the motion prescribed with only the leading and trailing edges produced no positive thrust during the downstroke. All the flexible cases reproduced the thrust production of the fully deformable fin. In the case of the rigid fin, a wake capture mechanism was observed that resulted in a small thrust increase just after the beginning of the downstroke. During the upstroke, when only the leading edge curvature is prescribed, as in the case with 4 control points, the peak thrust exceeds the fully deformable fin. Although the leading edge curvature was maintained to be the same between the 4 control point case and the fully deformable fin, the curvature in the mid chord region is much reduced when only the leading edge curvature is specified. This led to a smaller recirculation region on the upper surface of the fin producing extra thrust. From the point of view of lift production, we found that all of the cases with flexible fins performed in a similar manner except the fin controlled by just the leading and trailing edge points. In the case of the rigid fin, there was a substantial loss of lift during the upstroke. Therefore, the fish or a vehicle with rigid fin or a fin controlled by just the leading and trailing edge points would experience much more vertical excursions that one with a flexible fin.

ACKNOWLEDGEMENTS

This work was supported by ONR through a 6.2 project on Unsteady Hydrodynamics of Swimming Vehicles. The valuable discussions with Mr. Mark Westneat and Prof. Jefferey Walker of University of Southern Maine and Prof. Rainald Löhner of George Mason University throughout the course of this project is greatly appreciated. This work was supported in part by a grant of HPC time from the DoD HPC centers, ARL MSRC SGI-O2K and NRL SGI-O2K.

REFERENCES

Dickinson, M. H., Lehmann, F.-O. and Sane, S. P. (1999). Wing rotation and the aerodynamic basis of insect flight. *Science* **284**, 1954-1960.

Ellington, C. P., Van den Berg, C. and Willmott, A. P. (1996). Leading-edge vortices in insect flight. *Nature* **384**, 626-630.

Liu, H. and Kawachi, K. (1998). A numerical study of insect flight. *J. comp. Physics.* **146**, 124-156.

Ramamurti, R. and Löhner, R. (1992). Evaluation of an Incompressible Flow Solver Based on Simple Elements, *Advances in Finite Element Analysis in Fluid Dynamics*, FED **137**, Editors: Dhaubhadel, M. N. *et al.*, ASME Publication, New York, 33-42.

Ramamurti, R. and Sandberg, W.C. (2002a). A Three-Dimensional Computational Study of the Aerodynamic Mechanisms of Insect Flight, *J. Exp. Biol.* **205**, 1507-1518.

Ramamurti, R., Löhner, R., and Sandberg, W. C. (1994). Evaluation of a Scalable 3-D Incompressible Finite Element Solver, *AIAA-94-0756*, Washington, DC.

Ramamurti, R., Löhner, R., and Sandberg, W. C. (1995). Simulation of a Torpedo Launch Using a 3-D Incompressible Finite Element Flow Solver, *AIAA-95-0086*, Washington, DC.

Ramamurti, R., Löhner, R., and Sandberg, W. C. (1999). Computation of the 3-D Unsteady Flow Past Deforming Geometries, *Int. J. Comp. Fluid Dyn.*, 13, 83-99.

Ramamurti, R., Sandberg, W.C. and Löhner, R. (2000). Simulation of the Dynamics of Micro Air Vehicles, *AIAA-2000-0896*, Reno, NV.

Ramamurti, R., Sandberg, W.C., Löhner, R., Walker, J. A. and Westneat, M. W. (2002b). Fluid Dynamics of Flapping Aquatic Flight in the Bird Wrasse: 3-D Unsteady Computations with Fin Deformation, *J. Exp. Biol.* **205**, 19, 2997-3008.

Walker, J. A. and Westneat, M. W. (1997). Labriform Propulsion in Fishes: Kinematics of Flapping Aquatic Flight in the Bird Wrasse, *Gomphosus Varius.* (Labridae), *J. Exp. Biol.* **200**, 1549-1569.

Willmott, A.P. and Ellington, C.P. (1997). The mechanics of flight in the hawkmoth Manduca Sexta. II. Aerodynamic consequences of kinematics and morphological variation, *J. Exp. Biol.* **200**, 2723-2745.

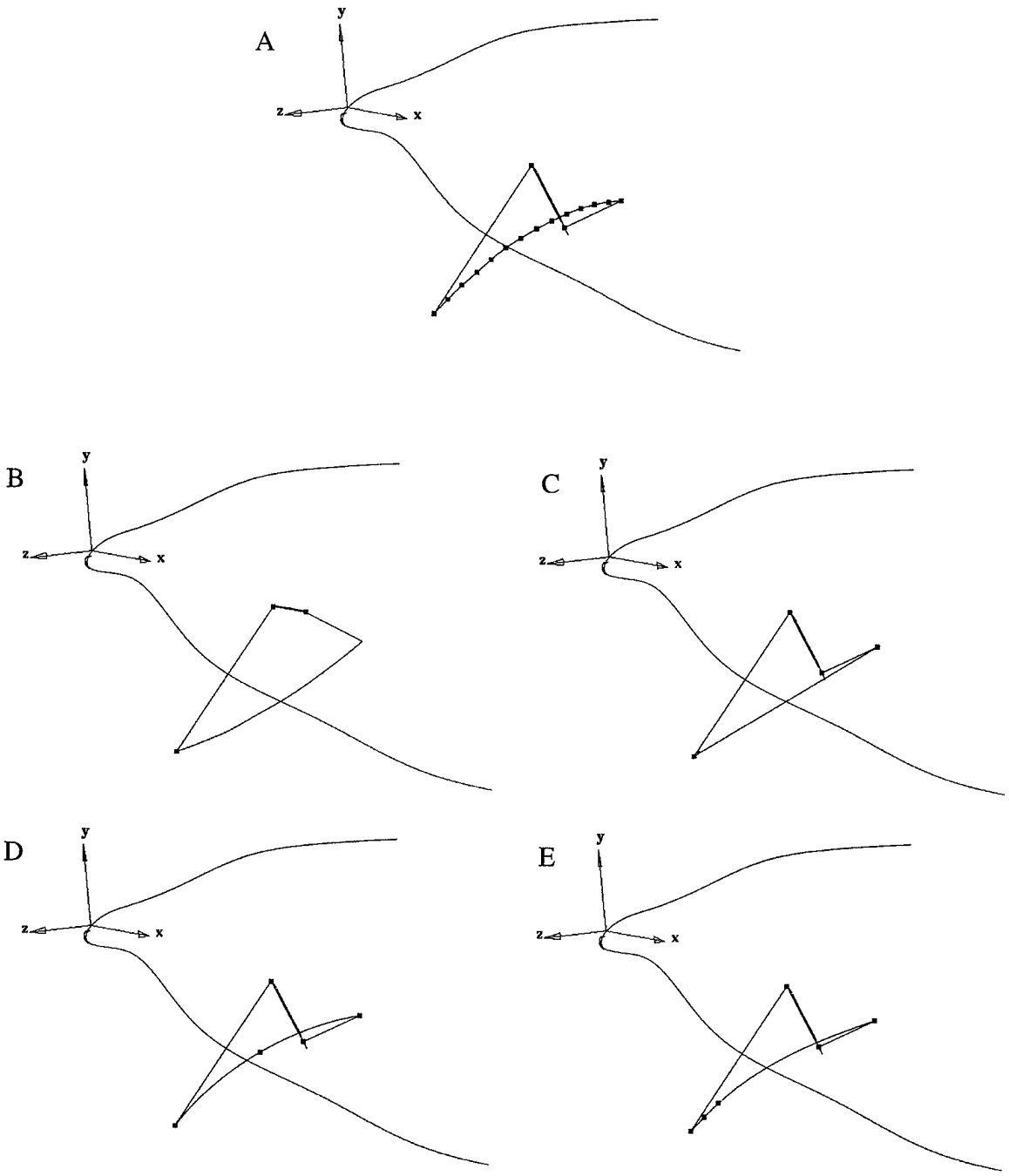

Fig. 1. Shapes of the fully deformable Bird-wrasse fin and modified fin at an instant when the fin is fully extended. (A) The experimentally observed deformable fin with 14 control points, (B) modified rigid fin with a control point on the leading edge and at the tip of the fin, (C) flexible fin with control points at the leading and trailing edges of the fin tip, (D) flexible fin with 3 control points, and (E) flexible fin with 4 control points closer to the leading edge.

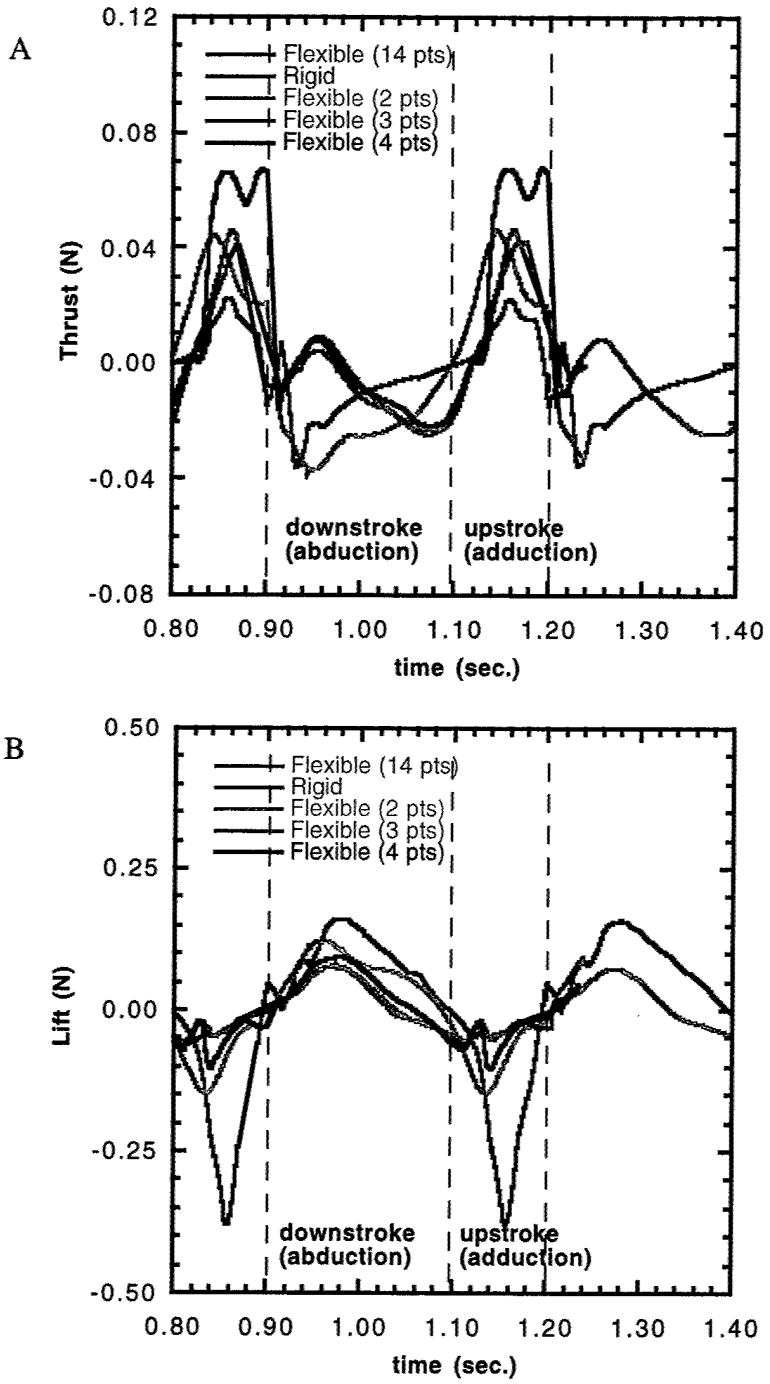

Fig. 2. Effect of fin flexibility on the time variation of (A) thrust and (B) lift forces.

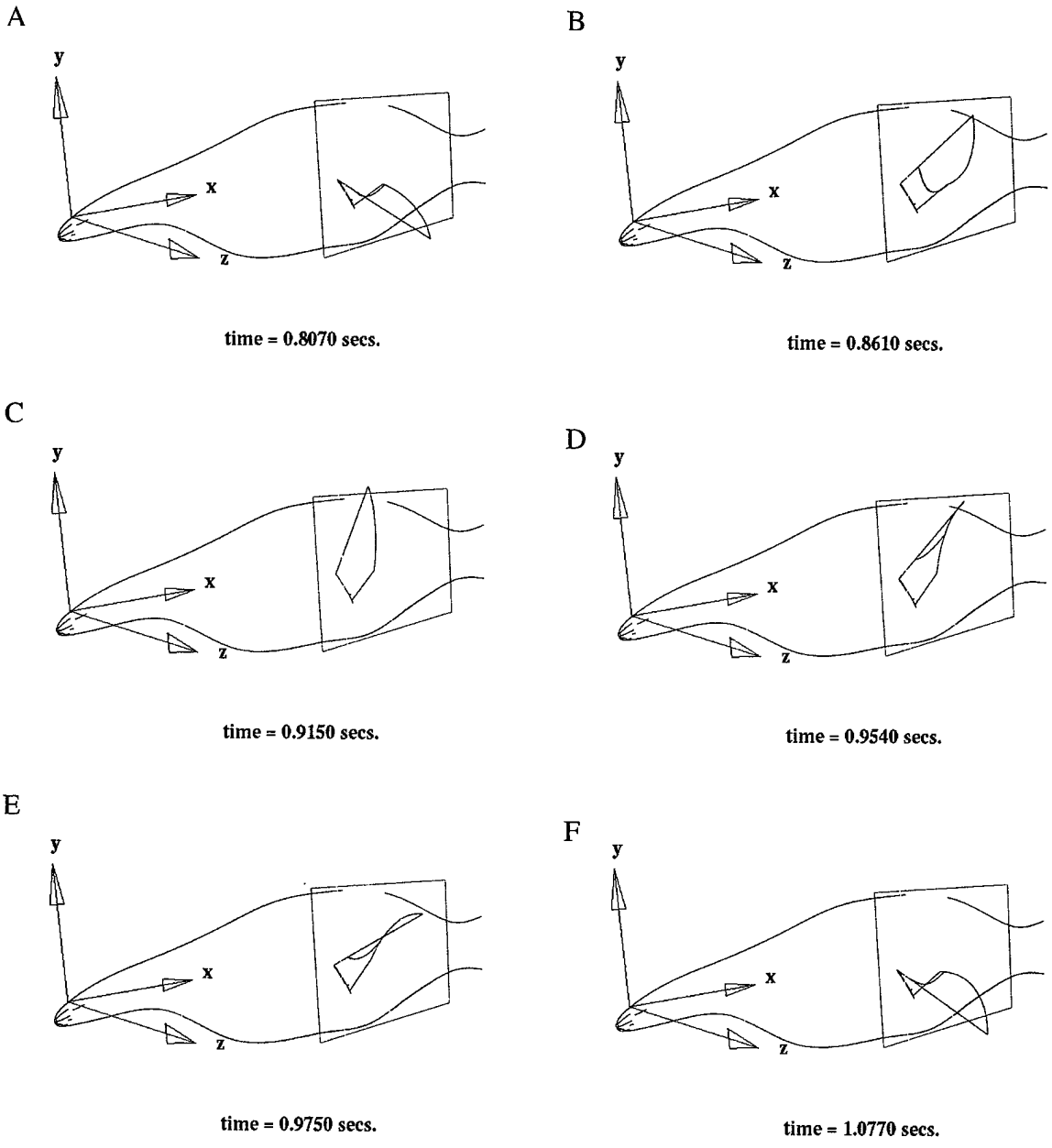

Fig. 3. Orientation of the Bird-wrasse and the pectoral fin during one cycle of flapping of the fin. The plane z = 1.5cm and the intersection of the fin with this plane are shown in red. The position of the fin at (A) the beginning of the upstroke, (B) during the mid upstroke, (C) beginning of the downstroke, (D and E) middle of the downstroke and (F) near the end of the downstroke are shown.

A

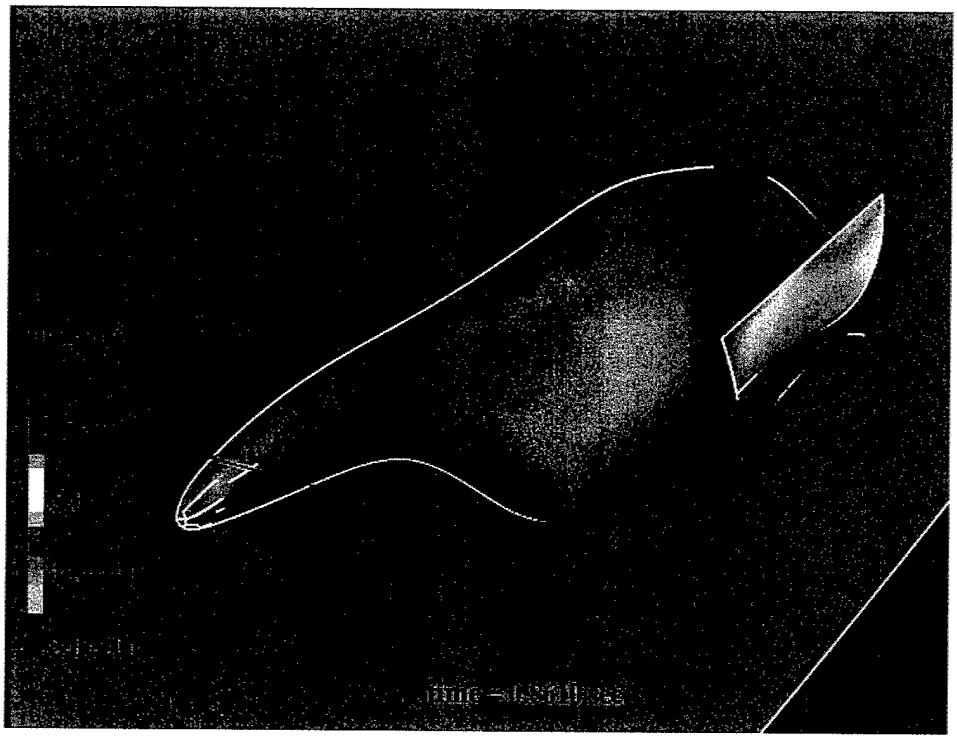

B

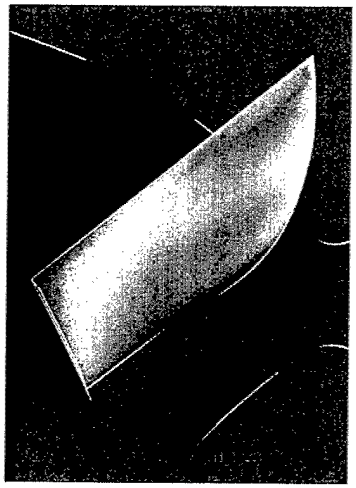

C

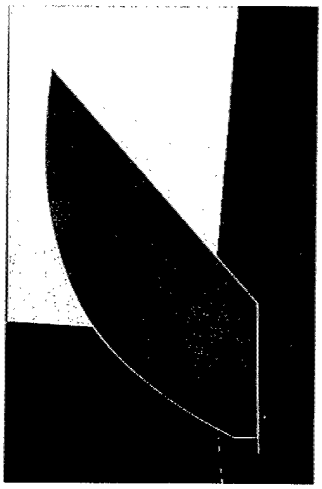

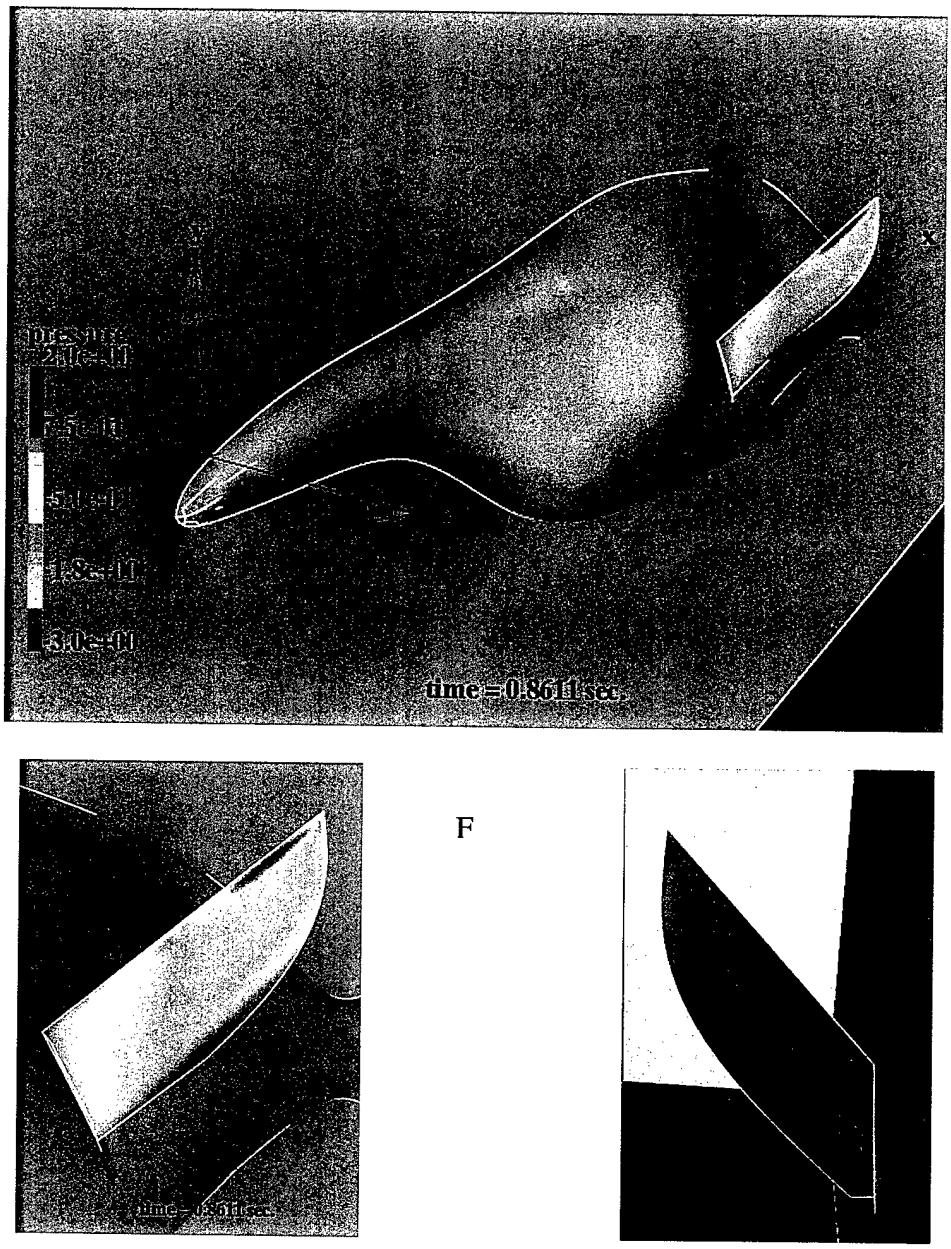

Fig. 4. Surface pressure distribution on the Bird-wrasse at an instant when the thrust is maximum during the upstroke. The pressure is non-dimensionalized with respect to the dynamic head of the mean tip velocity. (A-C) 14 control points were used to define the kinematics of the fin. (A) shows the orientation of the fin at t = 0.810 secs. and the pressure distribution on the surface of the Brid-wrasse. (B) Enlarged view from the front of the lower side of the fin. (C) Enlarged view from the back of the fin. (D-F) 4 control points were used to define the kinematics of the fin. (E) Enlarged view from the front of the lower side shows lower pressure compared to (B) and (F) view from the back of the upper side of the fin show higher pressure compared to (C), resulting in a higher thrust.

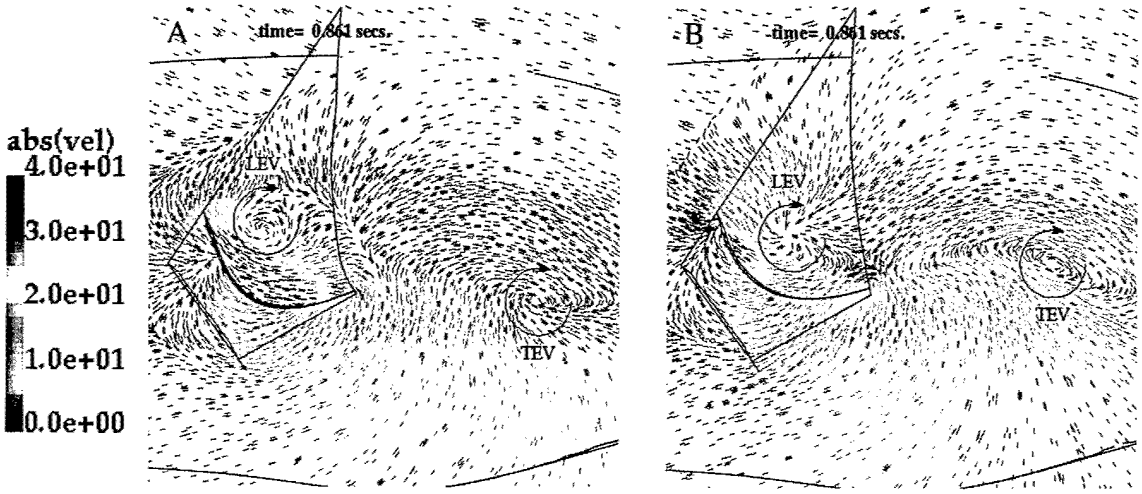

Fig. 5.Velocity vectors on a plane z = 1.5 cm at an instant t = 0.861 s, when the thrust production is maximum during the upstroke with fin kinematics prescribed with (A) 14 control points and (B) with 4 control points. The swimming velocity of the fish (45 cm s-1) is subtracted from the x component of the velocity and only the in-plane components are shown to reveal the vortical structures. LEV, leading edge vortex; TEV, trailing edge vortex.

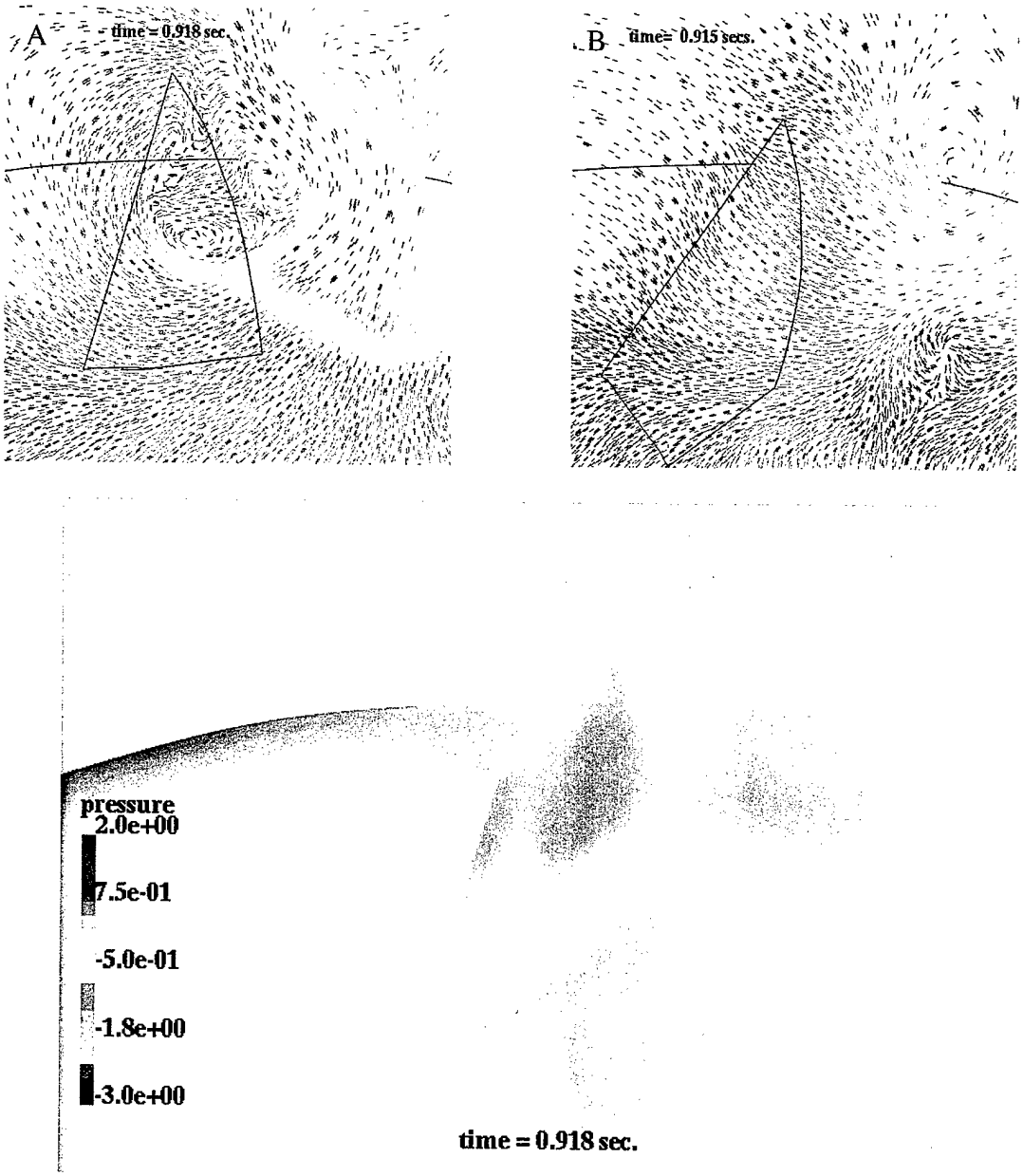

Fig. 6. Thrust production in the rigid fin just after stroke reversal, $t = 0.918$ s. (A) velocity vecors on a plane z = 1.5 cm, show vortices from the wake of the previous upstroke, (B) velocity vectors just after stroke reversal for the fully deformable fin showing the absence of the vortices in the fin region, and (C) pressure distribution on the lower side of the rigid fin showing higher pressure region due to the presence of the wake vortices.

A

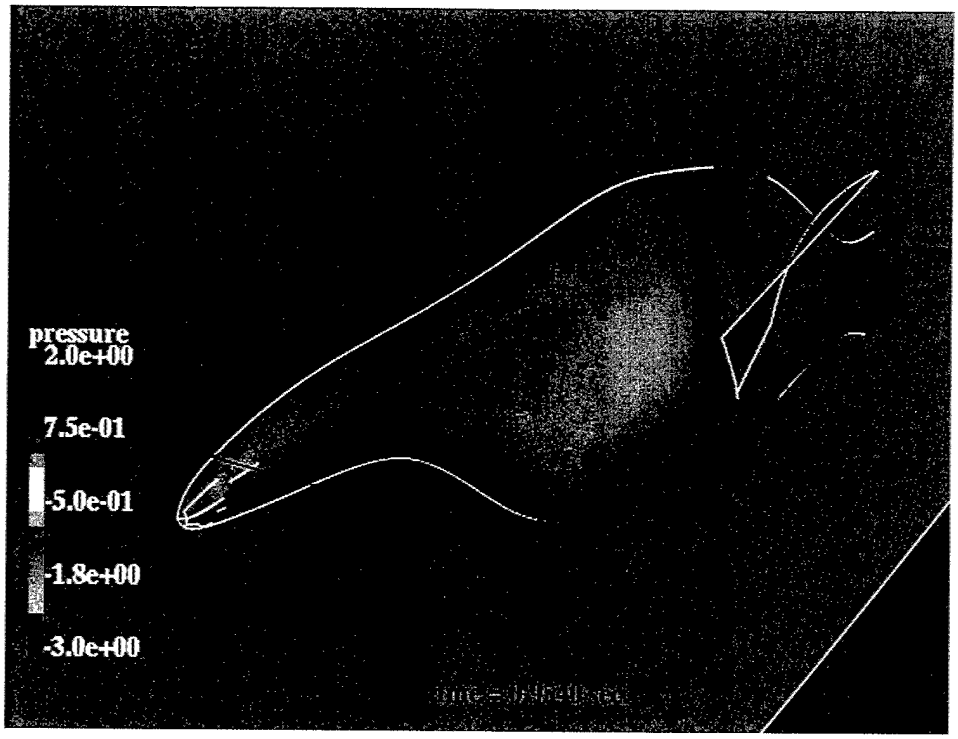

B

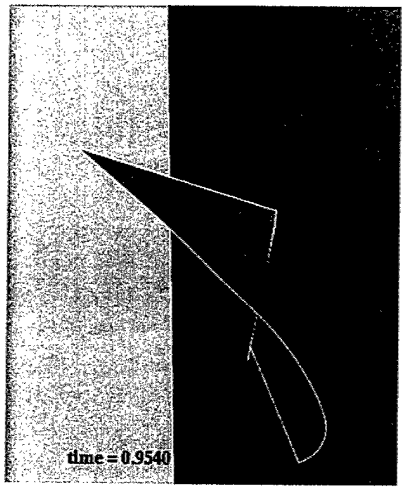

C

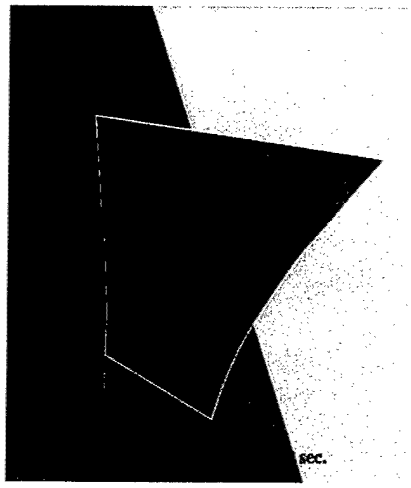

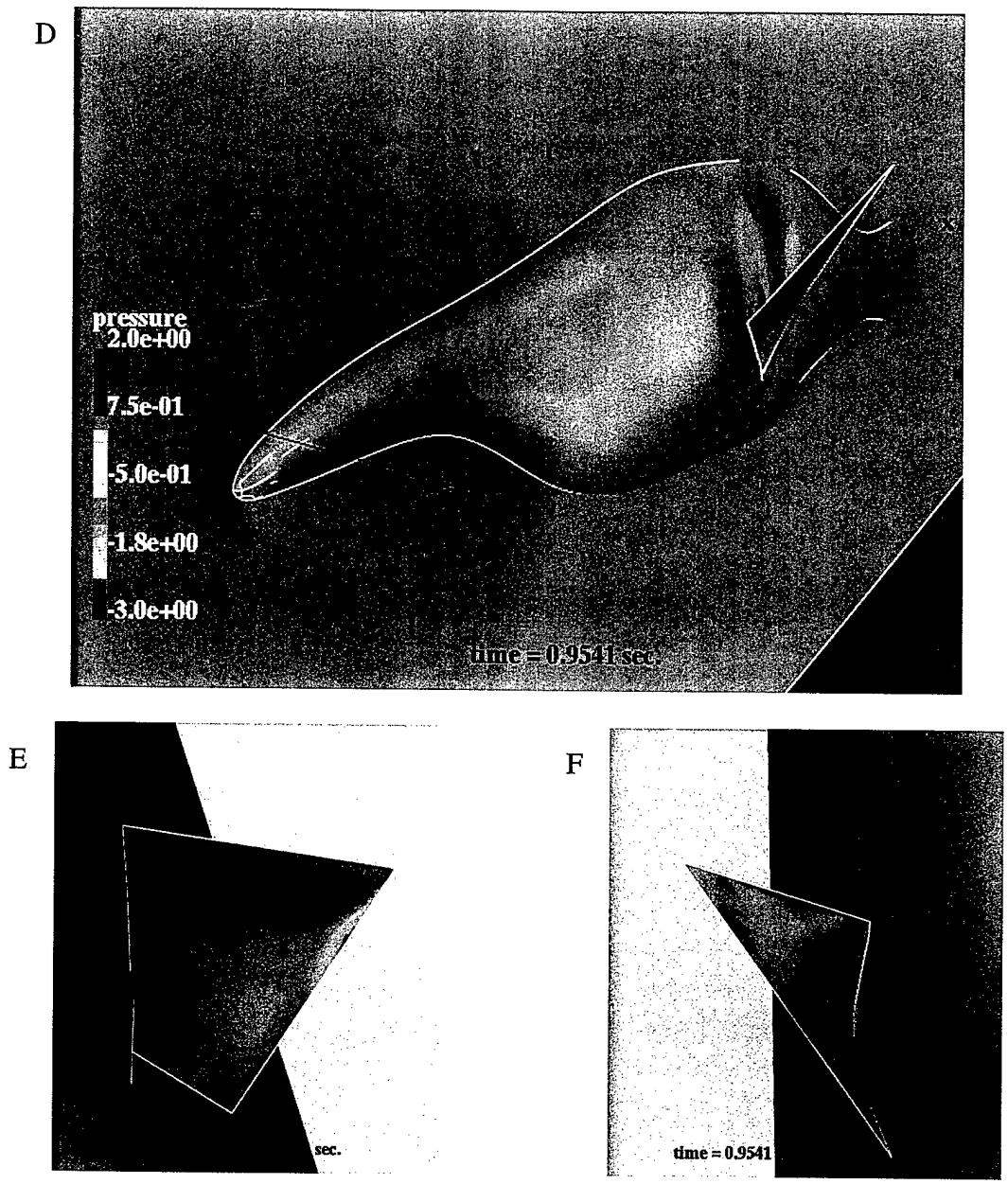

Fig. 7. Pressure distribution on the Bird-wrasse and its pectoral fin at t = 0.954 s during the downstroke, (A-C) when the thrust reaches maximum for the fully flexible fin and (D-F) when the thrust reaches a minimum for case with the fin kinematics prescribed by 2 control points.

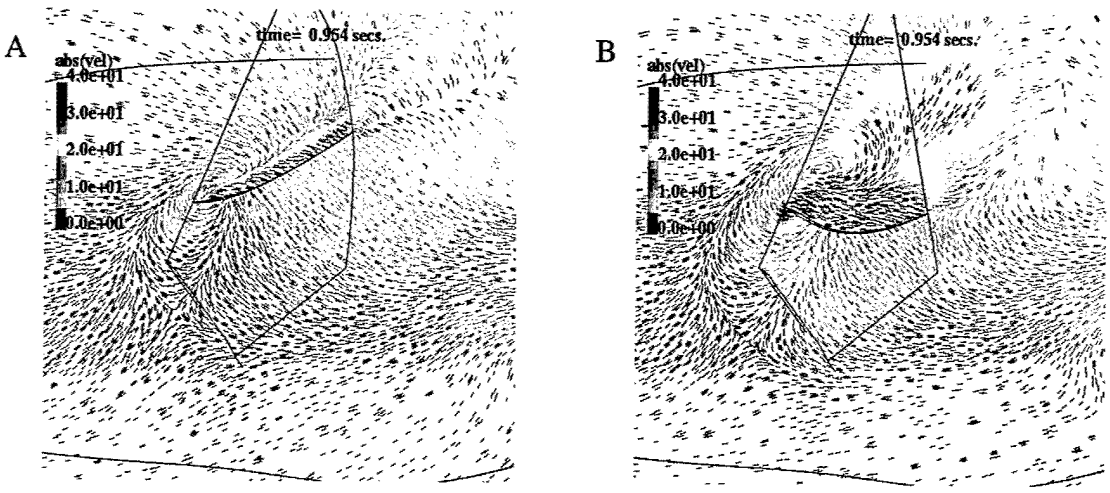

Fig. 8. Velocity vectors on a plane z = 1.5 cm at an instant t = 0.954 s, (A) when the thrust production is maximum during the downstroke with fin kinematics prescribed with 14 control points and (B) when the thrust production reaches a minimum with 2 control points. The swimming velocity of the fish (45 cm s-1) is subtracted from the x component of the velocity and only the in-plane components are shown to reveal the vortical structures. Although the leading and trailing edges in both case are prescribed in the same manner, the curvature in the 2 control point case (B) is pronounced in the middle of the fin, leading to a large recirculation, resulting in lower pressure on the upper surface.

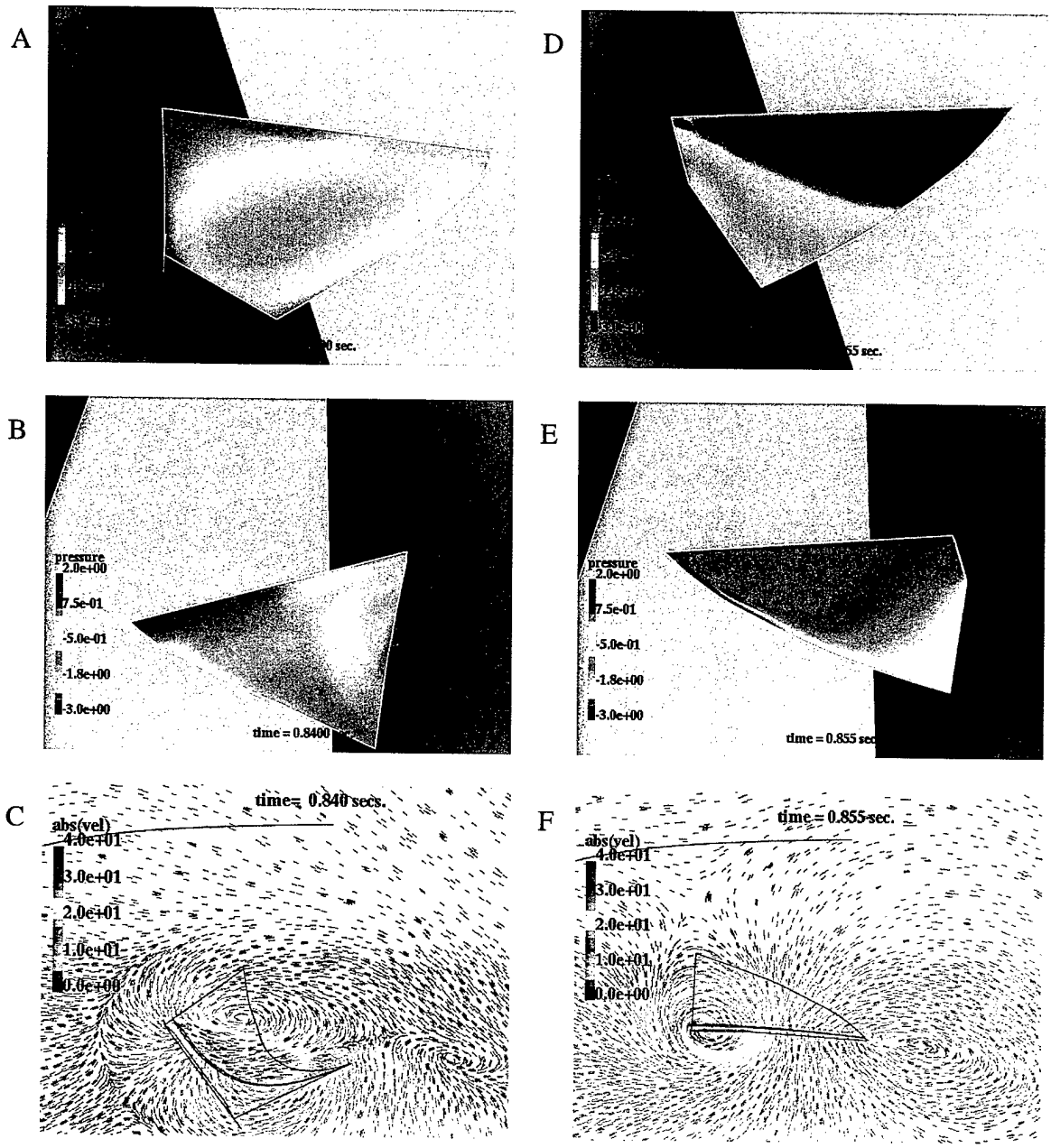

Fig. 9. Surface pressure contours on the pectoral fin and velocity vectors on a plane z = 1.5 cm at an instant when the lift is minimum during the upstroke for the rigid fin. (A-C) fully flexible fin; (D-F) rigid fin. pressure distribution on the lower surface viewed from the bottom(A, D) and on the upper surface viewed from the top (B, E). (C) Velocity vectors show a large recirculation on the upper surface, lowering the pressure and thus increasing lift when compared to (F) a fully attached flow in the rigid case.

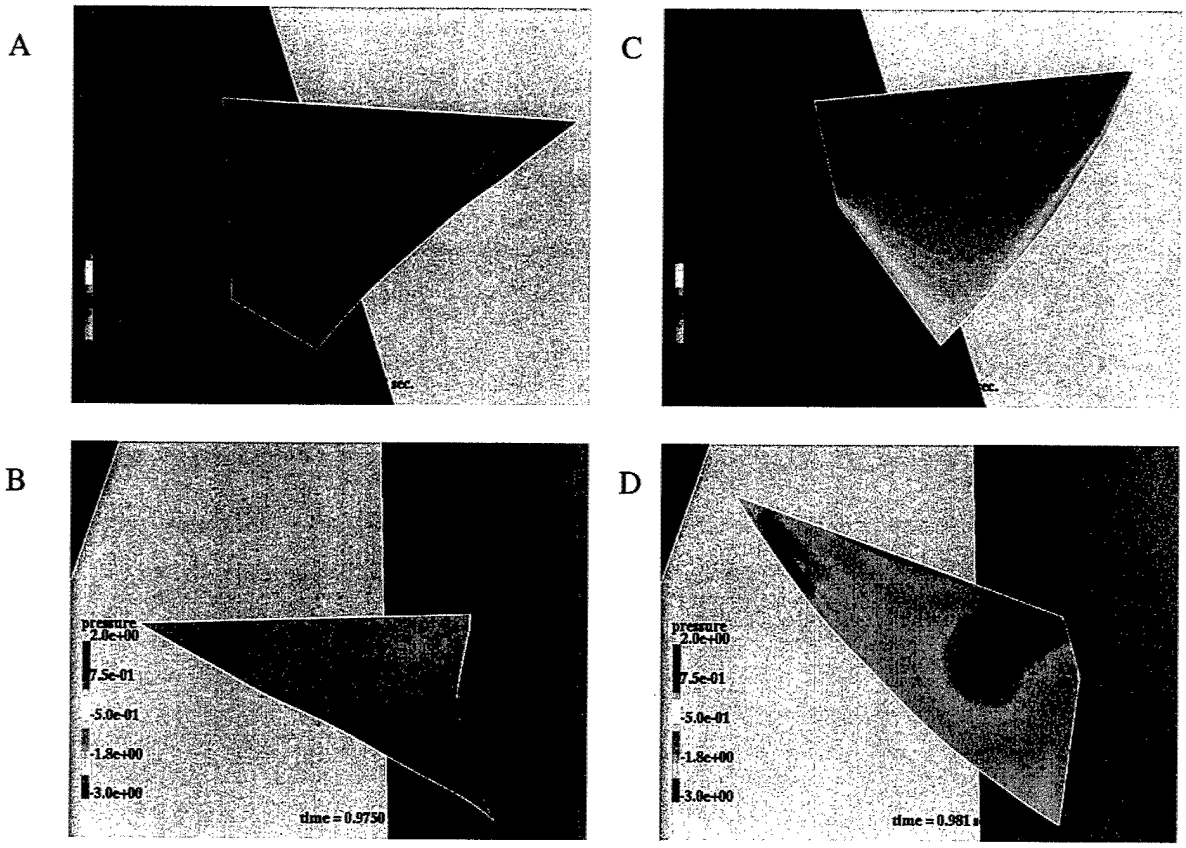

Fig. 10. Surface pressure distribution on the pectoral fin at an instant when the lift is near maximum during the downstroke, (A, B) for the fully flexible fin and (C, D) for the rigid fin. (C) Lower surface of the fin viewed from the bottom shows higher pressure at the distal edge of the fin and most of the lower surface when compared to (A) and the pressure on the upper surface is much lower for the rigid case (D) when compared to the fully flexible fin (B), resulting in a higher lift force.